Directly diode-pumped Colquiriite regenerative amplifiers

A. Isemann *, P. Weßels, C. Fallnich

Laser Zentrum Hannover e.V., Laserentwicklung, Hollerithallee 8, 30419 Hannover, Germany

Abstract

The Colquiriite crystals are attractive materials for directly diode-pumped femtosecond oscillators and amplifiers. Cr:LiSAF, Cr:LiS-GAF and Cr:LiCAF are for the first time directly compared for their use in regenerative amplifiers both experimentally and theoretically. A maximum pulse energy of 10 μJ was obtained at an absorbed pump power of 1.1 W. A review of the work is given including a Cr:LiSAF seed oscillator, outlining specific needs for seeding.
© 2005 Elsevier B.V. All rights reserved.

1. Introduction

The application of femtosecond pulses is being established outside laboratory environments, e.g., in materials processing or ophthalmology. For these areas of application, compact, efficient, and therefore directly diode-pumped systems offering pulse energies of several microjoules and a pulse duration of 150–200 fs are needed [1], as they are not available today.

The Cr^{3+}-doped Colquiriite crystals show very suitable properties for these aims. The crystals absorb pump light at wavelengths in the range from 600 to 700 nm, that is covered by the emission range of high-power laser diodes, and the broadband laser emission is in the near infrared spectral region centered between 780 and 850 nm. The gain bandwidth of approximately 200 nm suffices for generating sub-100 fs pulses.

The first directly diode-pumped Colquiriite regenerative amplifier was demonstrated by Melish et al. [2] and was based on Cr:LiSAF. In the same group, an amplifier based

on Cr:LiSGAF was realized, but with different laser diodes as pump source [3]. The first regenerative amplifier based on Cr:LiCAF was demonstrated by Isemann et al. [4].

The experimental setup of the work done so far by the different authors always differed somewhat, making it difficult to directly compare the properties of the Colquiriites for their use in a regenerative amplifier. Therefore, in this paper a systematic comparison under equal conditions is presented. With equal conditions the identical pumping arrangement and mode diameters, crystal size and absorption length is meant. In addition, a comprehensive theoretical modelling for an estimate of power scaling capabilities was carried out and is presented.

Efficient heat removal proves to be a critical issue. Thermal quenching, i.e., the temperature-dependent efficiency reduction, which was previously observed by Balembois et al. [5], has to be avoided. Thermal quenching occurs, e.g., with Cr:LiSAF starting at a temperature of 69 °C [6]. To reduce the temperature in the pumped volume, a novel arrangement was used. In this arrangement, the ellipticity of the cavity mode due to a single Brewster angled surface inside the resonator was matched to the pump-beam-geometry of the broad-area pump diodes. Using low-doped thin slab crystals the large surface to volume

---

* Corresponding author. Tel.: +49 511 27880.
  E-mail addresses: isemann@uni-bremen.de (A. Isemann), cf@lzh.de (C. Fallnich).

ratio of the pumped volume resulted in efficient heat removal and a reduced temperature and thus, thermal quenching was avoided. The description of the cw-operation of lasers using the Colquiriite amplifier geometry presented here was published earlier [7], where a cavity layout for thermal management was introduced in more detail.

As described later on, a pulse energy of 10 μJ was generated from a broad-area diode-pumped regenerative Cr:LiSGAF amplifier, which was limited only by the pump power available from broad area laser diodes nowadays. The further potential was estimated from the theoretical modelling.

The paper is organized as follows: In the following section, the Cr:LiSAF oscillator and a frequency doubled mode-locked Er-doped fiber laser are characterized as seed sources. Then, the setup and operation of the Cr:LiSAF, Cr:LiSGAF and Cr:LiCAF amplifier is described, followed by a theoretical modelling of the pulse energy and pulse build-up time, fitted to the experimental results. The power scaling capabilities are estimated from the model. Finally, the suitability of these three crystals for their use in a regenerative amplifier is compared.

2. Seed sources

2.1. Cr:LiSAF oscillator

A tuneable Cr:LiSAF oscillator was used for seeding of the Cr:LiSAF as well as the Cr:LiSGAF amplifier, since the wavelength of maximum gain is only 10 nm apart. The setup of the oscillator consisted of a standard X-type resonator, as displayed in Fig. 1. One arm contained a pair of fused-silica Brewster prisms spaced at 350 mm for dispersion compensation, the other arm contained a SESAM (semiconductor saturable absorber mirror) for mode-locking. The Cr:LiSAF crystal was positioned between two focusing mirrors with a radius of curvature of $R = -100$ mm. The folding angle of the arms was chosen to 8° for astigmatic compensation. The total resonator length was 1.49 m.

The mode-locking was started and stabilized by the SESAM, where the necessary fluence of the pulse on the SESAM (0.2–2 mJ/cm²) was obtained by a focusing mirror with a radius of curvature of $R = -100$ mm. A fine adjustment of the fluence was done by moving the SESAM along the optical axis and thus changing the radius of the cavity mode. The output coupler was located behind the prism

sequence, and an exterior prism sequence was used to recompress the spatial chirp of the beam. The crystal was pumped longitudinally by laser diodes through the folding focusing mirrors, which where coated highly transmissive (>94%) for the pump wavelength of 670 nm and highly reflective (>99.97%) for the laser wavelength. To compensate for the astigmatism introduced by traversing the folding mirror at an angle, a lens of the same radius of curvature was placed in front of the mirror. Collimation and focusing of the pump beam was done by two lenses of 90 mm focal length. The laser diodes were fast axis collimated with an emitter size of 1 μm × 50 μm and an output power of 350 mW each. The Cr:LiSAF crystal was doped at 1.5 at.%, with Brewster cut ends, a diameter of 4 mm and a length of 6 mm. The crystal was placed in a copper mount, which was thermo-electrically cooled to 16 °C. A knife edge was inserted between the last prism and the output coupler for tuning the emission wavelength of the oscillator.

2.1.1. Experimental results

The optimum output coupling (OC) was determined experimentally in the range of 1.5–2.7%. In Fig. 2, a characteristic curve is given for mode-locked operation and for cw-operation replacing the SESAM by a highly reflecting mirror. At higher intracavity losses, a slightly higher output coupling resulted in maximum output power. Because the SESAM has non-saturable losses, a slightly higher output coupling was used to give highest output power. In cw-operation at 2.2% of output coupling, 102 mW of output power were generated at 580 mW of absorbed pump power
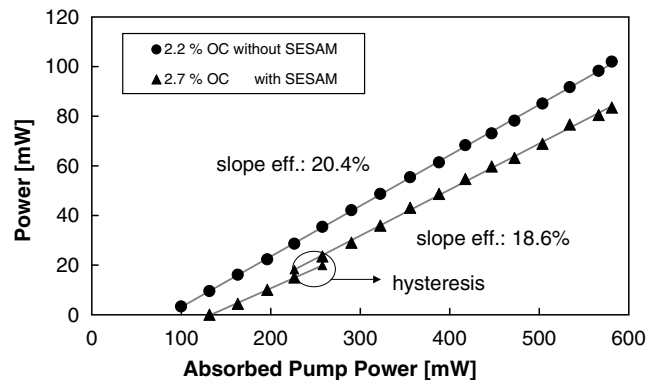

Fig. 2. Slope efficiency of the oscillator in cw-operation and mode-locked operation, details see text.
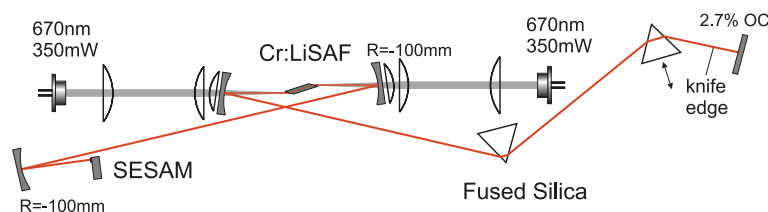

Fig. 1. Setup of the Cr:LiSAF oscillator. For details see text.

with a slope efficiency of 20.4%; in mode-locked operation at an output coupling of 2.7% the output power was 88 mW at a slope efficiency of 17.6%. The beam quality was measured to $M^2 < 1.07$ in the tangential direction, and $M^2 < 1.05$ in the sagittal direction. The transition to mode-locked operation was observable by a sudden increase in intensity due to the lower losses of the now saturated saturable loss and showed a hysteresis for increasing or decreasing the pump power [8].

An interferometric autocorrelation and the corresponding spectrum are depicted in Fig. 3. Since the spectrum showed a sech^2-shape, the pulse form in time is also sech^2-shape, related by a Fourier-transform, and the assumption of a sech^2-shape pulse is thus well justified. The FWHM (full width at half maximum) spectral width was 14.6 nm and the pulse duration 56 fs after deconvolution. Thus, nearly transform-limited pulses with a time–bandwidth-product of 0.33 were observed.

The pulse width was limited by the reflective bandwidth of the SESAM and the associated higher order dispersion arising at the edges of the highly reflecting wavelength regions. At wider spectra, higher order dispersion at the extreme spectral positions resulted in the generation of dispersive waves, which ultimately destabilized the soliton pulse. An example of the extra spectral peaks appearing due to the presence of dispersive waves is given in Fig. 4.

The limitation in minimal pulse width may also be seen from Fig. 5, where the measured pulse duration and bandwidth are displayed for an increasing amount of glass, and thus, decreasing negative group delay dispersion (GDD). According to theory, shortest pulses are obtained at a minimum of negative intracavity GDD [9].

While the spectral bandwidth increases with decreasing GDD, the pulse width reaches a steady value from a certain displacement value of the glass insertion. The non-decrease in pulse width at increasing bandwidth was attributed to the non-compensated higher orders of dispersion, which not yet destabilized the soliton to collapse into cw-operation, but resulted in dispersive waves.

For seeding an amplifier, clean femtosecond pulses as displayed in Fig. 3 without a background of dispersive
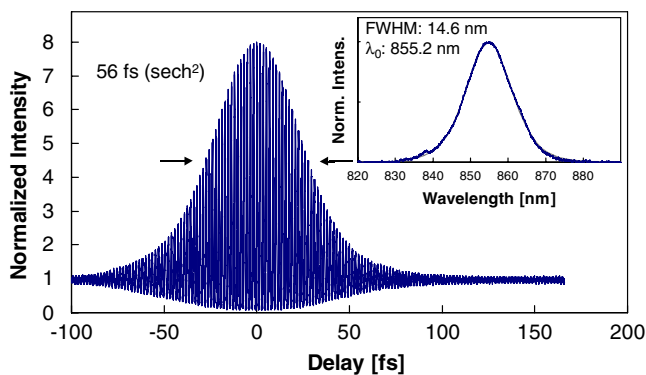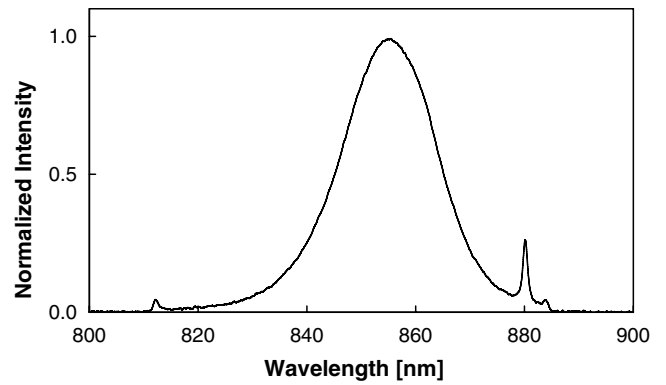

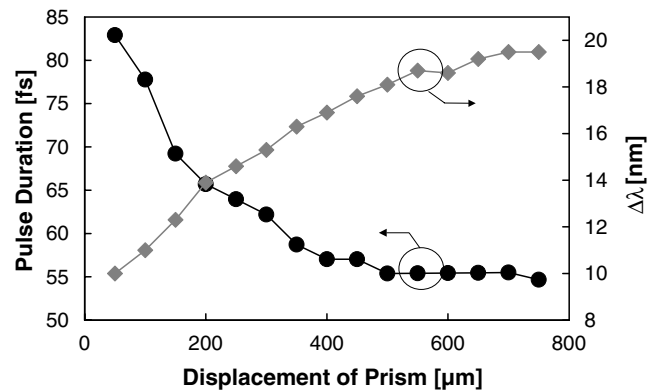Fig. 4. Appearance of additional spectral peaks due to formation of dispersive waves.

Fig. 5. Reduction of the pulse duration and increase of the bandwidth by increasing the amount of prism-glass and thus reducing the GDD.

waves are preferred, since the dispersive wave constitutes a background of longer pulses [10], which would also get amplified and would take away gain for the femtosecond pulse.

2.2. Frequency doubled Er-doped fiber Laser

To seed the Cr:LiCAF amplifier, a seed source emitting pulses in the wavelength range around 780 nm is necessary. In this wavelength range another seed source besides a Cr:LiCAF or Ti:sapphire oscillator exists – a frequency doubled mode-locked Er-doped fiber laser. This laser constitutes a much more compact, reliable and maintenance-free seed source compared to a Ti:sapphire oscillator. The setup of the fiber laser (see Fig. 6) was already described in an earlier publication [11], and is summarized here again for completeness.

An Er-doped normal-dispersion active fiber was closed to a ring cavity using an anomalous-dispersion SMF1528 and Flexcor 1060 fiber for dispersion compensation. Polarization controllers for alignment of the cavity internal state of polarization and an isolator were used as well for unidirectional operation as for separation of the output. A telecommunication laser diode with an emission wavelength of
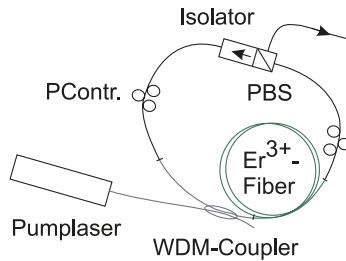

Fig. 3. Interferometric autocorrelation and spectrum of the Cr:LiSAF oscillator.

Fig. 6. Setup of the mode-locked Er-doped fiber laser.

Fig. 8. Intensity autocorrelation and spectrum of the frequency doubled pulse of the fiber laser.

980 nm was used to pump the Er-doped fiber via a wavelength division multiplexing coupler.

At 150 mW of pump power 23 mW of fundamental average output power at 1550 nm at a repetition rate of 57 MHz were generated. The autocorrelation pulse width of the chirped output pulses was measured to be 100 fs with a multi-peaked spectrum reaching from 1500 to 1610 nm as shown in Fig. 7.

For frequency conversion of the 1550 nm radiation to the near infrared, we used chirped periodically poled lithium niobate (CPPLN) crystals [12]. By linearly increasing the width of the poled domains (chirp) a longer crystal can be used and a wider spectral range can be frequency converted compared to a non-chirped crystal. Simultaneously, a phase modulation was imposed onto the frequency doubled pulse. Starting with an almost unchirped fundamental pulse, the frequency doubled pulse was stretched. Injection of this pre-stretched pulse into the amplifier together with additional material dispersion inside the amplifier eliminated the need for a conventional pulse stretcher to reduce the peak pulse intensity before injection in comparison to conventional pulse amplification schemes [13]. Consequently, this allowed a more compact setup with no reduction of seed energy due to losses from gratings.

The used CPPLN was 10 mm in length and the domain period varied linearly from 17.9 to 19.9 μm. At a fundamental input power of 23 mW and focusing the input beam with a lens of 35 mm focal length into the CPPLN, 2 mW of second-harmonic output power were obtained. A spec-
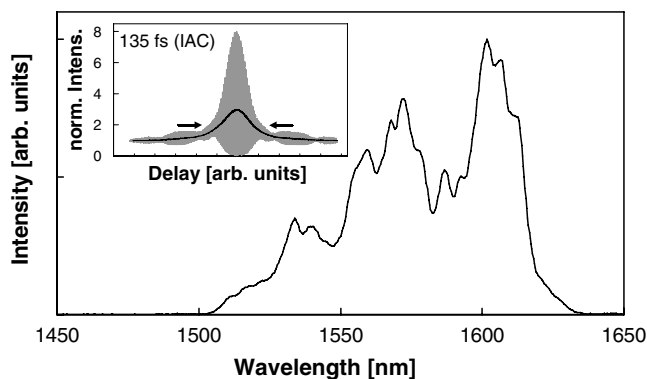
trum and autocorrelation of the frequency doubled radiation is depicted in Fig. 8.

The autocorrelation of the second-harmonic pulse implied a chirped pulse length of 600 fs (sech^2). The spectral width was fitted to 10.7 nm with a sech^2-shape.

3. Regenerative amplifiers

3.1. Experimental setup

The setup of the Colquiriite amplifiers consisted of a V-shaped resonator utilizing at one end a flat-Brewster cut crystal of dimensions 4 mm × 1 mm × 5 mm ($W \times H \times L$). The doping of the crystals was chosen such that the absorption length was the same within 10%. The flat side of the crystal was coated highly reflective for the lasing wavelength and highly transmissive for the pump wavelength. As shown in Fig. 9, for each side the beams of two broad area pump laser diodes (emitter: 1 μm × 100 μm, fast axis collimation) were polarization-coupled and focused into the crystal providing up to four times 500 mW of pump power at 670 nm.

The ellipticity of the cavity mode due to a single Brewster surface together with only spherical focal elements inside the resonator was optimized by the ABCD-matrix formalism [14] to match the measured elliptical pump beam profile. The first demonstration of this concept was reported in [15]. The concept of an elliptical cavity mode but with the use of cylindrical elements to match an elliptical pump beam was first introduced by Kopf et al. [16] when pumping a Cr:LiSAF laser with a laser diode array. The high reflectivity resonator mirrors used in this setup exhibited a reflectivity of >99.97%.

For trapping a seed pulse in the amplifier cavity and coupling out the amplified pulse, a Pockels cell and thin film polarizer (TFP) combination was employed. For the Cr:LiSAF and Cr:LiSGAF amplifier, a Medox Pockels cell driver was used; for the Cr:LiCAF a differential driver consisting of two FET (field-effect transistor) high voltage switches was used to drive the Pockels cell (KD*P). This scheme allowed fast rising and falling edges of the high

Fig. 7. Interferometric and intensity autocorrelation (inset) and spectrum of the fundamental pulse of the fiber laser.
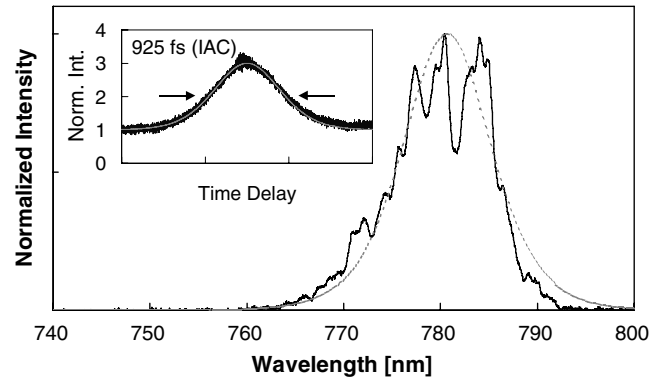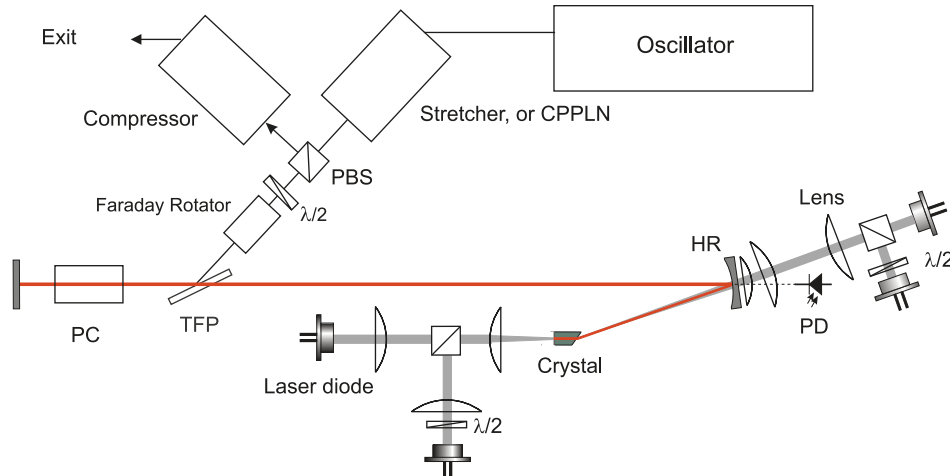
Fig. 9. Setup of the amplifiers, details see text (PD, photo diode; HR, high reflector; PBS, polarizing beam splitter; PC, Pockels cell).

voltage as well as a long holding time of more than 5 μs, which was needed in case of the Cr:LiCAF amplifier. Both drivers showed switching times of approximately 4 ns, sufficiently below the cavity round trip time of 5.4 ns. A more detailed description of the switching scheme can be found in [11,17]. The mode matching of the oscillators to the amplifier was done by two closely spaced lenses of appropriate focii ($f = 2000$ mm) for fine tuning the matching. The incoming beam was separated from the exiting beam by an optical diode consisting of a Faraday rotator, half-wave plate and polarizing beam splitter.

A leaking beam from a high reflectivity mirror focused onto a fast photodiode (rise time <200 ps) was used to observe the pulse build-up inside the resonator. Another leaking beam was directed through a multi-mode fiber into an optical spectrum analyzer (ANDO) to measure the spectral bandwidth.

For the Cr:LiSAF and Cr:LiSGAF amplifier, a commercial grating stretcher and compressor (Spectra Physics) employing a grating constant of 1500 grooves/mm was used for chirped pulse amplification. In the Cr:LiCAF amplifier presented here, due to the large number of round trips (~370) inside the amplifier, enough phase modulation due to material dispersion was accumulated to sufficiently stretch the seed pulses such that no critical peak power occurred. Pulse compression was done by gold coated reflection gratings (1200 grooves/mm) in double pass configuration. The details of this setup are described in [11].

The laser was first aligned in cw-operation. After adjusting the cw-cavity, the output coupler was replaced by a high-reflectivity mirror. The Pockels cell (KD*P) and the thin film polarizer were installed and adjusted for maximum leaking cw-power from the high-reflectivity end mirror with a power meter. After optimizing the cw-operation, the Pockels cell was oriented to yield static quarter-wave retardation while applying a quarter-wave voltage to allow for the trapping of a seed pulse or the build-up of a Q-switched pulse. Before seeding, the amplifier was

optimized in Q-switched operation for minimum pulse build-up time.

The pulse width was measured with a single shot autocorrelator using a BBO crystal for second-harmonic generation and a CCD-array for spatially resolved detection of the frequency doubled radiation.

3.2. Experimental results

3.2.1. Cr:LiSAF

In the Cr:LiSAF amplifier, a 1.5 at.% Cr^{3+}-doped crystal was used. The scattering loss was determined in an earlier experiment to less than 0.14% [7]. All experiments were carried out at a repetition rate of 1 kHz unless otherwise noted.

After optimizing the amplifier in Q-switched operation, the seed beam of the Cr:LiSAF oscillator was directed into the amplifier and adjusted for shortest pulse build-up time and complete seeding, i.e., no Q-switched signal noted underneath the circulating pulse from the photo diode signal. About 80 pJ of pulse energy were used to seed the amplifier. A comparison of the Q-switched and the seeded operation is given in Fig. 10, where the trace of a leakage of the pulse through the resonator mirror measured with a
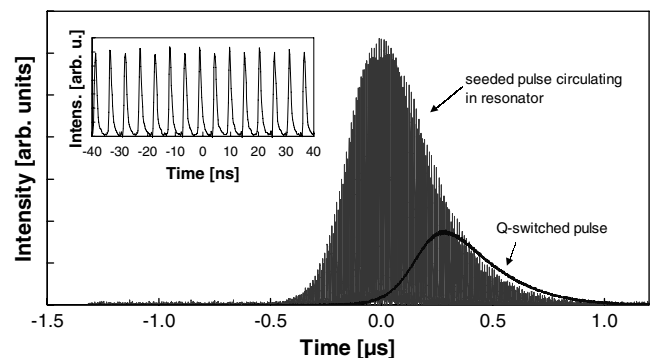

Fig. 10. Comparison of the circulating seeded pulse to Q-switched operation with an enlarged view of the seeded pulse in the inset.

photo diode is depicted. The longer pulse build-up time of the Q-switched pulse is due to the build-up from noise, compared to the build-up from the photons of the seed pulse. No sign of a Q-switched background is visible, as can be seen from the enlargement in the inset of Fig. 10. The spacing of the peaks of 5.4 ns fitted the round trip time of the resonator. The slight change in amplitude was due to the photodiode and the sampling rate of the digital oscilloscope (aliasing effect). When coupling the amplified pulse out of the cavity, a contrast ratio of 1:200 for pre- to main-pulse was achieved.

Fig. 11 shows the output energy versus absorbed pump power for Q-switched as well as seeded operation. The pulse build-up time is given for the seeded operation only, for the clarity of the graph. The pulse energy from Q-switched operation was recorded directly behind the thin film polarizer, whereas for seeded operation the energy was measured behind the optical diode. This may be one reason for reduced energy by an amount of 0.5 μJ due to additional losses from the optical diode. The different slope efficiencies might be attributed to the broader spectral width of the pulse in seeded operation versus Q-switched operation causing slightly higher losses per round trip in some components, e.g., in the Pockels cell or the thin film polarizer, which accumulated over 185 round trips to a measurable amount. The measured pulse energy of 9 μJ is the highest recorded to date from pumping with broad area diodes.

The spectrum of the seed pulse, which was tuned to the peak of the spectral amplification as well as of the amplified pulse are given in Fig. 12. A narrowing of the spectral width of the amplified pulse was observed.

The reduction of the spectral bandwidth from 15 nm of the seed pulse to 7 nm of the amplified pulse was due to the well known gain narrowing. Different spectral components experience a different gain, and since the wings of the spectrum are less amplified compared to the peak of the spectrum in this wavelength range, the resultant spectrum has undergone a narrowing.
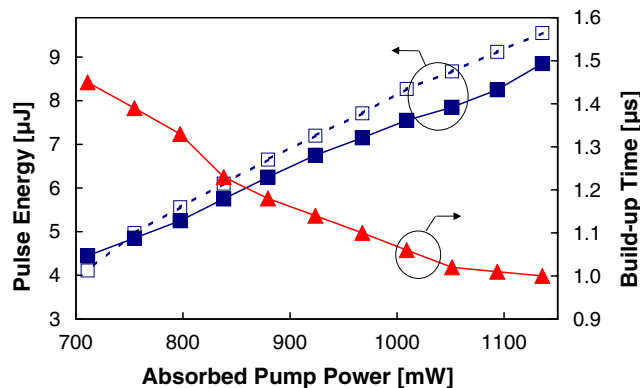

Fig. 11. Pulse build-up time and pulse energy versus absorbed pump power for Q-switched (open markers) and seeded operation (filled markers). For seeded operation, also the pulse build-up time is displayed.
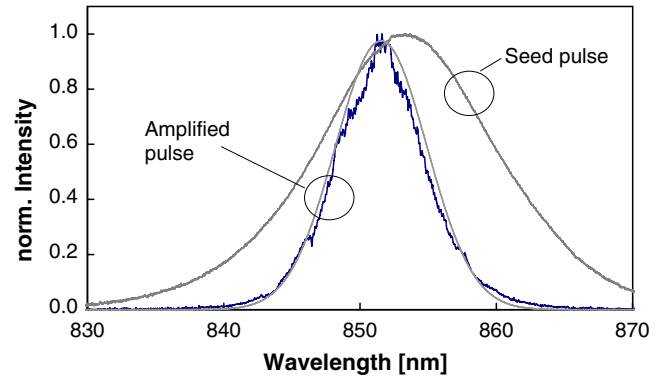

Fig. 12. Spectrum of the seed pulse and the amplified pulse with sech²-fit for the Cr:LiSAF regenerative amplifier.

The extend of gain narrowing can be calculated with the following simple formula given by Rouyer [18]:

$$\Delta\lambda = \frac{\Delta\lambda_0}{\sqrt{1 + \ln(G)\left(\frac{\Delta\lambda_0}{\Delta\lambda_{\mathrm{Fluo}}}\right)^2}}, \tag{1}$$

where $\Delta\lambda_0$, $\Delta\lambda$ and $\Delta\lambda_{\mathrm{Fluo}}$ denote the spectral width of the incident pulse, of the amplified pulse and the spectral width of the amplifying medium, whereas G is the gain.

The gain narrowing of the amplifier was calculated recursively from this formula, adjusting the initial small signal gain of 1.127 and initial spectral bandwidth as given before for each round trip. The small signal gain for the different round trips was calculated from the theoretical modelling described in Section 3.3. The spectral width of the amplifying medium was taken as 196 nm. The result of this calculation of the gain narrowing was in excellent agreement within 5% of the experimental result.

The pulse duration of the amplified pulse was measured by a single shot autocorrelation. Having a maximum pulse fluence of 0.09 J/cm², the amplifier was operated far below the saturation fluence of 4.8 J/cm² [19], thus, a linear amplification of the pulses was given. The B-Integral [14] was calculated to $B < 0.04$, thus, a nonlinear phase distortion could be excluded. The amplified pulses could be compressed to 173 fs. The bandwidth was 7.15 nm from a sech² fit. The resulting time–bandwidth-product of 0.51 implied non-transform-limited pulses. Using all the available bandwidth, pulses of 107 fs should have been possible. The cause of the non-perfect compression was non-compensated third order dispersion. During approximately 200 round trips, in combination with the compression gratings, a TOD of the order of 2×10^6 fs³ was accumulated. Imposing a TOD of this order on a transform-limited pulse of 107 fs duration results in a pulse duration of approximately 170 fs, as was calculated numerically. Thus, the non-transform-limited compression of the pulses could be traced to the grating stretcher and compressor used, in which the gratings of equal grating constants could not compensate the additional TOD imposed onto the pulse by material dispersion.

Many applications benefit from an increased repetition rate. Several commercial amplifiers offer a repetition rate of 1–5 kHz. The Medox Pockels cell driver was specified up to 20 kHz. When a regenerative amplifier is pumped continuously, the full pulse energy may be extracted up to a repetition rate equal the inverse of the upper state life-time. At higher repetition rates, the energy storage level is not fully repumped, and thus the maximum obtainable pulse energy decreases at a given amount of pump power. For Cr:LiSAF, the upper state lifetime is 67 μs [19], from which a decreased pulse energy is expected above a repetition rate of 15 kHz. This behavior was experimentally observed by Mellish et al. [20]. From the measurements conducted in our experiment, a clear decrease was observed already above 6 kHz, as is depicted in Fig. 13.

Fig. 13 shows the normalized pulse energy versus repetition rate for different temperatures of the crystal mount. The tilt of the Pockels cell was not adjusted for higher repetition rates, and above 17 kHz no extraction of the pulse was possible. From these measurements, a thermal influence from the laser crystal could be excluded, since the effect did not depend on the temperature. Rather, this effect was due to a change in the high voltage at the Pockels cell with increased repetition rate. This was examined external to the resonator, where for repetition rates greater than 6 kHz an increasing deviation of the high voltage from the quarter-wave high voltage was observed. Thus, using a Pockels cell driver delivering high voltage independently on the repetition rate, full pulse energy up to 15 kHz should be obtainable.

3.2.2. Cr:LiSGAF

The setup of the Cr:LiSGAF amplifier was the same as described before except for the crystal, which was a 2 at.% Cr^{3+}-doped LiSGAF crystal. The scattering loss was again determined in an earlier experiment to less than 0.14% [7]. Since the maximum spectral amplification of Cr:LiSGAF is shifted only 10 nm towards shorter wavelengths compared to Cr:LiSAF, the same dielectric components were used. The Cr:LiSAF oscillator was used as tunable seed source.

All measurements were again performed at 1 kHz unless otherwise noted.

A maximum pulse energy of 10.5 μJ was measured directly behind the thin film polarizer at an absorbed pump power of 1130 mW. A curve of the pulse energy versus absorbed pump power is displayed in Fig. 14, open markers, where the pulse build-up time is given again for the seeded operation only, for the clarity of the graph. In the next step, the seed beam was adjusted into the amplifier. The wavelength of the oscillator was tuned to 845 nm and an average power of about 8 mW corresponding to 80 pJ was injected into the amplifier.

The pulse energy and build-up time versus absorbed pump power are given in Fig. 14, closed markers. The energy was measured behind the optical diode. The amplifier showed the same general behavior as the Cr:LiSAF amplifier. The measured pulse energy in the seeded case was somewhat lower compared to the Q-switched operation. This was attributed to the additional losses of the optical diode, while the slight difference in slope efficiency was attributed to the same reason (larger loss at broader operation bandwidths) as for the Cr:LiSAF amplifier.

As in the case of Cr:LiSAF gain narrowing was observed. The bandwidth of 11.5 nm of the injected pulse was reduced to 6.9 nm of the amplified pulse as displayed in Fig. 15. The calculated reduction of the bandwidth according to formula (1), using as initial small signal gain a value of 1.111 from the theoretical modelling, reproduced the measured values within 10% in very good agreement. Again, a bandwidth of the amplifying medium of 196 nm was taken for the calculation. The pulse duration was measured with a single shot autocorrelation as 170 fs. The resulting time–bandwidth-product was 0.5. The limitation of the pulse duration to non-transform-limited compression was attributed to non-compensated third order dispersion, which was caused by using gratings of the same grating constants in the stretcher and compressor, as previously in the Cr:LiSAF amplifier.

The maximum fluence of the amplified pulse inside the amplifier crystal was approximately 0.09 J/cm^2, which
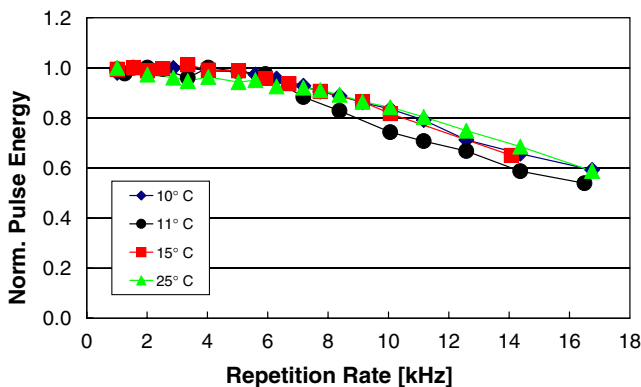
Fig. 13. Maximum pulse energy in dependence on the repetition rate for various cooling temperatures of the crystal mount.
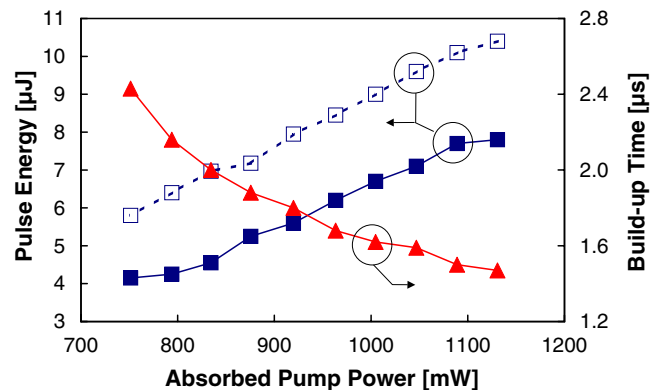
Fig. 14. Pulse build-up time and pulse energy versus absorbed pump power for Q-switched (open markers) and seeded operation (filled markers). For seeded operation, also the pulse build-up time is displayed.
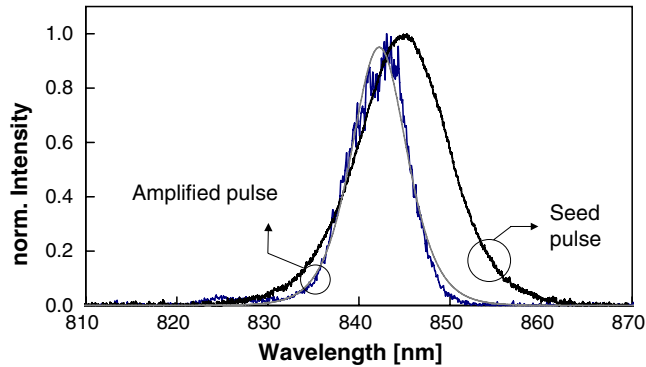
Fig. 15. Spectrum of the seed pulse and the amplified pulse with sech²-fit curve for the Cr:LiSGAF regenerative amplifier.

was well below the saturation fluence of 7.2 J/cm² of Cr:LiSGAF [19], thus, no influence onto the chirped pulse amplification from saturation was inferred. The B-Integral was calculated to $B \leqslant 0.04$, which corresponded to the value for the Cr:LiSGAF amplifier and also gave no indication for nonlinear effects.

As in the case of the Cr:LiSAF amplifier, also the Cr:LiSGAF amplifier could not be operated at full pulse energy above a repetition rate of 6 kHz, which is depicted in Fig. 16. This was due to the shortcoming of the Pockels cell driver used as already described in the previous section. For Cr:LiSGAF, the repetition rate up to which the upper lasing level is pumped to saturation is approximately 12.5 kHz. The difference in the slope of the pulse build-up time occurring at approximately 12.5 kHz visible in Fig. 16, dashed lines, was attributed to not fully pumping the energy storage level to saturation at higher repetition rates, and thus a lower gain.

3.2.3. Cr:LiCAF

In the setup of the Cr:LiCAF amplifier, a 3.5 at.% Cr^{3+}-doped crystal was used. Due to the shorter emission wavelength, the dielectric mirrors and the thin film polarizer were exchanged for components centered at 780 nm. The scattering loss of the crystal was measured as <0.28% [7]. The first operation of this type of amplifier was reported
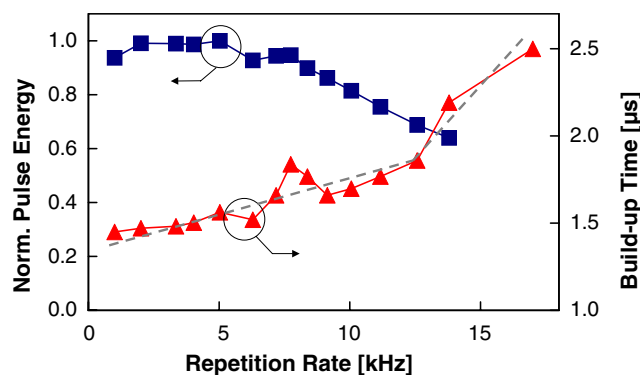
from us in [4,11], and the main results are summarized here.

A graph of the pulse energy and pulse build-up time versus absorbed pump power is displayed in Fig. 17 for Q-switched operation.

A maximum pulse energy of 8.2 μJ was obtained. A spectrum of the seed pulse and the amplified pulse are shown in Fig. 18 with a single shot autocorrelation in the inset.

The pulse duration was measured as 252 fs with a time–bandwidth-product of 0.6. The non-transform-limited compression was again due to the non-compensated third order dispersion, since the dispersion from material as well as from the grating compressor exhibited the same sign and thus, was not compensated. Third order compensation mirrors, which would mitigate this effect, were not available in this experiment. The spectral width of the seed pulse was reduced to 5.8 nm of the amplified pulse partly because of spectral clipping on the short wavelength side from the thin film polarizer. Although the pulse was mainly stretched by material dispersion during the round trips, the calculated B-Integral of $B < 0.7$ was significantly below the critical value of 3–5 [14]. Thus, a nonlinear phase modulation could be excluded. This can also be seen from the fact, that the spectral dip at approximately 783 nm of the
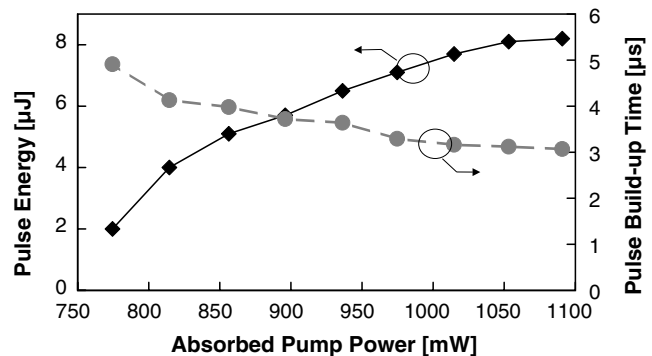

Fig. 17. Pulse build-up time and pulse energy versus absorbed pump power for Q-switched operation with Cr:LiCAF.

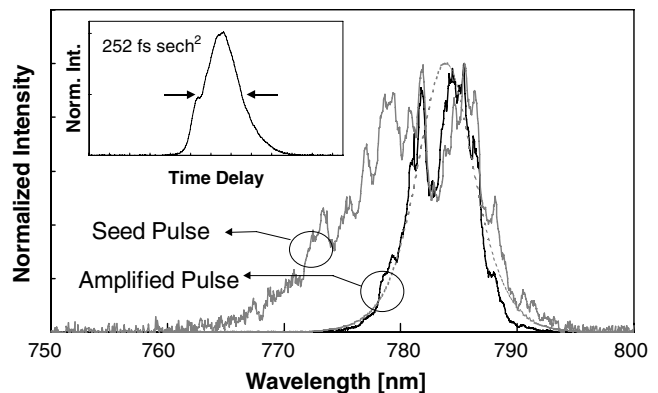Fig. 16. Pulse build-up time and pulse energy versus absorbed pump power for Q-switched operation with Cr:LiSGAF.

Fig. 18. Spectra of the seed pulse, the amplified pulse and a sech²-fit with a single shot autocorrelation in the inset with Cr:LiCAF.

seed spectrum was still present in the amplified spectrum. Nonlinear processes, such as self-phase-modulation would have filled the gap with additional spectral components. The maximum fluence of the pulse inside the crystal was about 0.09 J/cm^2, well below the saturation fluence of 18.2 J/cm^2 and thus, not inducing nonlinear effects.

Since the used FET Pockels cell driver only allowed a maximum repetition rate of 2 kHz, the repetition rate of about 6 kHz due to the upper state lifetime of 170 μs [19] up to which full pulse energy can be extracted could not be experimentally explored.

3.3. Numerical modelling and comparison

A numerical modelling of the amplification was carried out to compare the three Colquiriite crystals under identical conditions as well as their potential in power scaling in regenerative amplifiers.

3.3.1. Description of the amplifier equation

To describe the amplification of a pulse with a finite duration, the Frantz–Nodvik equation was used [21], which is given in Eq. (2). This model neglects spontaneous emission under the assumption, that the pulse duration and the time of flight through the amplifying medium are small compared to the lifetime of the upper laser level. This assumption is certainly fulfilled for the investigated amplifying medium

$$J_{out} = J_{Sat} \ln \left\{ 1 + e^{\eta \cdot g_0} \left[e^{\frac{J_{in}}{J_{Sat}}} - 1 \right] \right\}. \tag{2}$$

In the equation, J_{in} denotes the incident pulse fluence, $J_{Sat} = hc/\lambda\sigma$ the saturation fluence of the amplifying medium (h: Planck's constant, c: speed of light, λ: lasing wavelength, σ: emission cross-section), $g_0 = J_{Sto}/J_{Sat}$ the small signal gain and J_{Sto} the stored energy (density).

The effect of excited state absorption (ESA) reduces the available small signal gain, because a part η_{ESA} of the photons in the upper laser level is absorbed by higher lying levels and is lost for the amplification process. This was taken into account by introducing a factor $\eta = 1 - \eta_{ESA}$ with which the small signal gain was multiplied. The stored energy (density) J_{Sto} was calculated from the stored pump energy E_{abs}, the area A of the pump beam and the quantum defect $Q = \lambda_P/\lambda_L$ according to

$$J_{Sto} = \frac{E_{abs}}{A} \frac{\lambda_P}{\lambda_L}, \tag{3}$$

where $\lambda_{P,L}$ denotes the pump and lasing wavelength, respectively.

Eq. (3) multiplied by the cavity mode area describes the amplification of a single pass. To calculate the amplification of a regenerative amplifier, this equation has to be applied iteratively with the output energy of the nth pass taken as the input energy of the $(n + 1)$th pass, reduced by the passive losses. The stored energy of the upper laser level has to be reduced by the energy extracted in the nth

pass. A new small signal gain for the $(n + 1)$th pass is calculated accordingly.

The modelling of the amplifier was conducted for Q-switched operation, for which the pulse build-up time and pulse energy could be experimentally accessed easily. To describe the beam profile of the model, a rectangular distribution for the pump beam as well as the cavity mode was chosen. This beam profile resembled on the one hand the beam profile of the pump diodes much better than a Gaussian distribution, and on the other hand this accelerated the numerical calculation considerably. Therefore, fast results were obtained, which described the experiment nevertheless well concerning the pulse build-up time and output energy. For the intended frame, the full development of the model was therefore unnecessary. To fit the experimental energies to the model, a factor of the order of unity was introduced for the values from the model.

3.3.2. Comparison of the modelled and experimental results

The energy stored inside the crystal was calculated from the absorbed pump energy multiplied by the upper state lifetime. This corresponded to a saturation of the stored pump energy, valid up to a repetition rate $R_{Rep} = \frac{1}{\tau_{life}}$, where τ_{life} denotes the upper state lifetime. To define the pulse fluence, two Gaussian beam radii were used to calculate the rectangular area of the distribution. As starting value for the sum of passive losses, the experimental value of 2.5–4% obtained from a Findlay–Clay plot [22] in cw-operation was used. The amplification was started from noise photons of the energy 5×10^{-19} J, which corresponds to two photons of spontaneous emission. The pulse build-up time was not sensitive to the exact number of noise photons in the range of one to ten photons. The excited state absorption was taken as 35% for Cr:LiSAF [23], as 27% for Cr:LiSGAF [23], and as 26% for Cr:LiCAF [24]. All other crystal parameters were taken as given in the previous sections.

The model was fitted to the experimental data of the Cr:LiSAF amplifier using the above parameters as starting values. The best fit was obtained for a mode area of 49 μm × 68 μm and a passive loss of 2.66% per round trip. The fit of the axes of the rectangular pump mode corresponded to a fit to the distribution of the pump diodes. The used passive loss matched the measured experimental value within 10%. Following, the number of round trips were calculated for lower pump powers, where the asymmetric change of the beam profile of the two axes was taken into account.

The calculated data points (small markers) and the corresponding experimental data points (large markers) are displayed in Fig. 19. Both curves fit well. The fit of the mode radii obtained for the Cr:LiSAF amplifier was also used for both other amplifiers and was not changed. As fit parameter for experimental data of the other two crystals *only* the passive losses were used. The curve for Cr:LiSGAF was calculated with a loss of 4.06% per round trip and is also depicted together with the experimental data in Fig. 19. The excellent agreement shows that a suitable
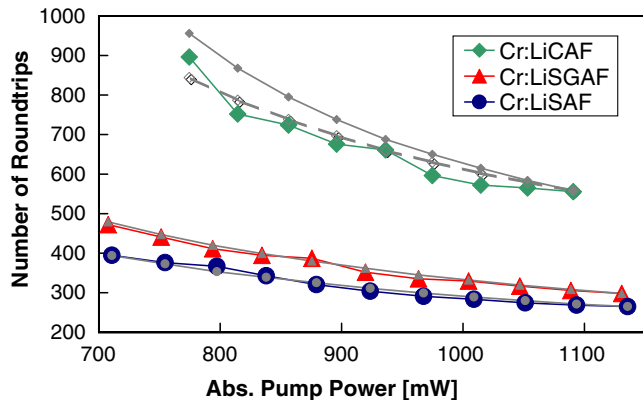
Fig. 19. Comparison of the experimentally obtained number of round trips (large dark symbols) with the number obtained from the model (small light gray symbols) in dependence on the absorbed (abs.) pump power for the three amplifiers; dashed line: calculation assuming 40% ESA instead of 26% for Cr:LiCAF. Details see text.
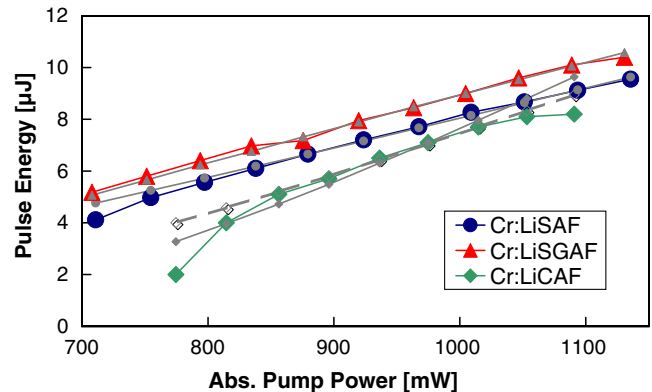

Fig. 20. Comparison of the experimentally obtained pulse energy (large dark symbols) with the energy obtained from the model (small light gray symbols) in dependence on the absorbed (abs.) pump power for the three amplifiers; dashed line: calculation assuming 40% ESA instead of 26% for Cr:LiCAF. Details see text.

theoretical description was found where for a different amplifying crystal simply the material specific input parameters had to be changed with the loss as the only variable parameter.

Adjusting the model to the experimental data of the Cr:LiCAF amplifier at highest pump power, a relatively high passive loss of 6.16% had to be used, which was not justified by the experimentally obtained value in the range of $3.5 \pm 0.5\%$. Also, at reduced pump power the curve for the experimental data did not fit as well to the calculated date points (closed symbols) compared to the other two crystals, as can be seen in Fig. 19. This may be due to the fact, that the value of the excited state absorption cited in the literature is not valid for the doping level of the crystal used in this experiment, as discussed in [7].

In that publication, the regenerative amplifier was operated as cw-laser, and a differential slope efficiency of 49% was obtained. To reduce the slope efficiency from its theoretical limit of 89% [25], an excited state absorption of 40% would have to be assumed. For a comparison, this value of the excited state absorption was entered into the model, the value of the passive loss was adjusted accordingly and a theoretical curve for the pulse build-up time was calculated. These data points are also displayed in Fig. 19 (open symbols). This curve fit much better to the experimental data, and also the used value of the passive loss of 3.96% was in the range of the values used for the two other amplifiers.

In Fig. 20, the theoretical curves of the pulse energy versus absorbed pump power are depicted which fit well to the experimental data of the Cr:LiSAF and Cr:LiSGAF amplifier.

In case of the Cr:LiCAF amplifier, a deviation of the theoretical values from the experimental data was observed, which already occurred for the pulse build-up time. Again, a much better fit was obtained when using an excited state absorption of 40% in the model. The essential result from the measurements of the pulse energy versus absorbed pump power is that the pulse energy had

the greatest increase with increasing pump power for Cr:Li-CAF, compared to the other two crystals. In fact, the absolute pulse energy was not higher at the available pump power of broad area diodes, but the output pulse energy can be expected much higher at pump powers available from, e.g., diode bars, which makes this material preferably for a power scaling.

3.3.3. Modelling under identical boundary conditions

Although Cr:LiSGAF exhibits a by 8% lower amount of ESA compared to Cr:LiSAF, a significantly higher output energy could not be measured. The reason being the higher passive losses. This becomes apparent when calculating data from the model using identical boundary conditions and same fit parameters for all three crystals. Identical boundary condition shall be understood in this case as identical mode radii, pump power, passive losses as well as equal number of start photons for the amplification process. The result of these calculations assuming a passive loss of 3% is depicted in Figs. 21 and 22. It becomes clear
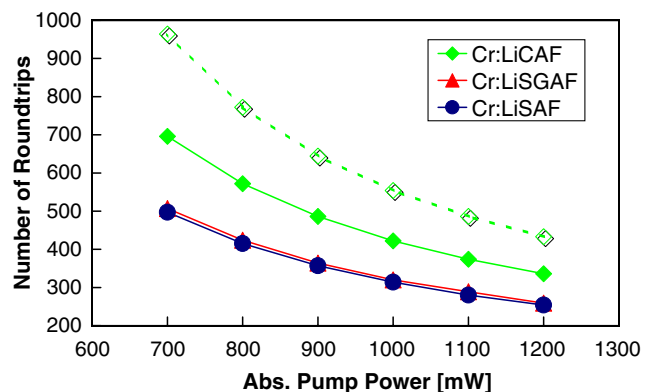

Fig. 21. Modelling of the number of round trips in dependence on the absorbed (abs.) pump power using identical conditions for the three amplifiers; note: curves for Cr:LiSAF and Cr:LiSGAF lie on top of each other; dashed line: calculation assuming 40% ESA for Cr:LiCAF.
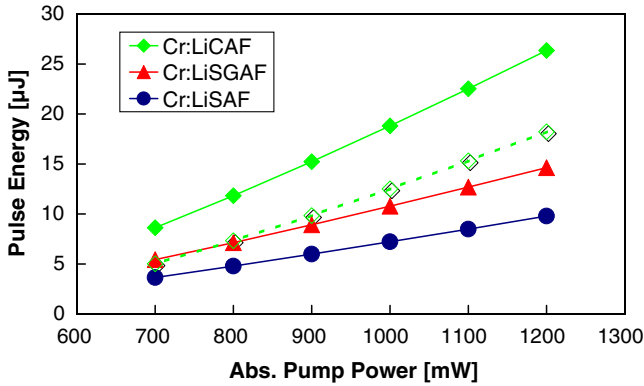
Fig. 22. Modelling of the pulse energy in dependence on the absorbed (abs.) pump power using identical conditions for the three amplifiers; dashed line: calculation assuming 40% ESA instead of 26% for Cr:LiCAF. Details see text.
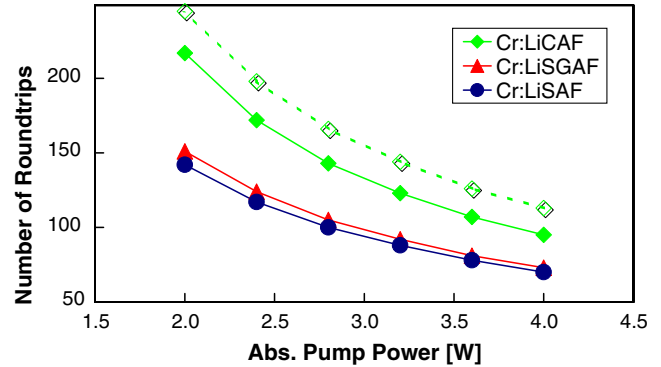

Fig. 23. Modelling of the number of round trips in dependence on the absorbed (abs.) pump power for a power scaling of the three amplifiers; dashed line: calculation assuming 40% ESA instead of 26% for Cr:LiCAF. Details see text.
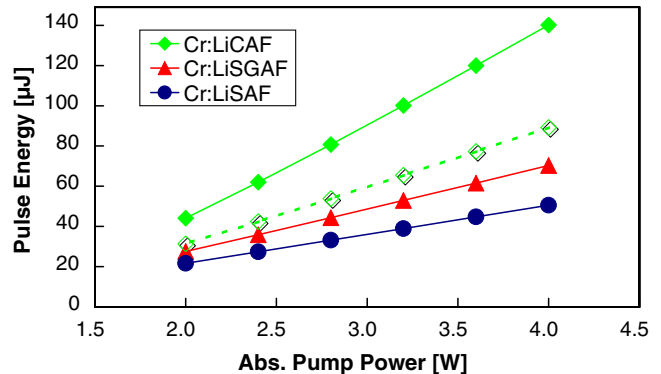

Fig. 24. Modelling of the pulse energy in dependence on the absorbed (abs.) pump power for a power scaling of the three amplifiers; dashed line: calculation assuming 40% ESA instead of 26% for Cr:LiCAF. Details see text.

from Fig. 22, that under these conditions, Cr:LiSGAF would have yielded a higher pulse energy compared to Cr:LiSAF. Furthermore, Cr:LiCAF yields an absolute higher pulse energy. At the same passive loss, the lower gain due to the stimulated emission cross-section was more than compensated for by the smaller quantum defect and the larger amount of stored energy due to the longer upper state lifetime. This remained valid even assuming an ESA of 40%.

The necessary number of round trips nevertheless stayed larger compared to the other two crystals due to the smaller gain, which becomes apparent from Fig. 21. In case of the Cr:LiSAF and Cr:LiSGAF, the effects from a different saturation fluence, different emission cross-section and losses due to ESA merely compensated each other. This resulted in an almost equal number of round trips necessary for the calculated maximum amplified pulse energy.

3.3.4. Modelling of power scaling

Furthermore, the model was used to simulate a power scaling with the V-resonator amplifier design. This was done under the assumption that the same brightness would be available at 670 nm like with diodes emitting at 808 nm. With these, an output power of approximately 1.6 W from an emitting aperture of 1 μm × 100 μm is obtained. Using a total of four diodes, about 4 W of absorbed pump power would be available. The calculations were done using all parameters from the fit to the experimental data for the three different crystals, since the power scaling was intended to be as close to experimental conditions as possible. Results from [7] indicate, that thermal quenching does not yet occur at these pump powers using the cavity design described here.

In Figs. 23 and 24, the number of round trips and the maximum energy are displayed, respectively, for an absorbed pump power between two and four Watts. For Cr:LiSAF, a maximum pulse energy of 50 μJ was reached, for Cr:LiSGAF 70 μJ and for Cr:LiCAF 140 μJ. To take also into account that Cr:LiCAF could exhibit an ESA

of 40%, the calculation was also performed with this value, which resulted in a pulse energy of 89 μJ. Again this shows the better suitability of Cr:LiCAF for higher pump powers, even when a possibly higher ESA is taken into account or higher losses as fitted from our experiment.

As can be seen from Fig. 23, the number of round trips necessary was reduced to 70 for Cr:LiSAF or Cr:LiSGAF when calculating with potentially four Watts of absorbed pump power, compared to 185 from the experiment pumping with only 1.2 W of absorbed pump power. This would reduce the accumulated dispersion of second and third order, which would result in less non-compensated third order dispersion by about 60% at recompression and consequently, in a shorter pulse duration of about 20% and the associated smaller time–bandwidth-product.

Thus far, the power scaling was viewed under the aspect of extracting the largest amount of pulse energy. For keeping the efficiency of the Colquiriite crystals, the temperature inside the pumped volume must be kept under the critical temperature for thermal quenching. Considerations have been given in a previous paper [7] with the estimation, that Cr:LiSAF and Cr:LiSGAF can be pumped with up to

3 W and Cr:LiCAF with up to 13 W of absorbed pump power – a range covering the pump powers used in the model for power scaling here.

4. Conclusion

In this work, three Colquiriite crystals were tested for their use in a regenerative amplifier. The experimental setup allowed for the first time a direct comparison. This was due to identical experimental conditions, such as pump configuration, crystal size, absorption length, resonator design, etc.

The highest amplified pulse energy at the available pump power from broad area diodes of 10.5 μJ was experimentally achieved with Cr:LiSGAF as the active material. Only a somewhat smaller pulse energy of 9.5 μJ was reached with Cr:LiSAF. The Cr:LiCAF amplifier generated 8.2 μJ of pulse energy. This energy was smaller compared to the other amplifiers, but the slope of the energy versus absorbed pump power was higher.

These results were reproduced in a theoretical modelling where Cr:LiSAF and Cr:LiSGAF showed very similar behavior, whereas Cr:LiCAF had a higher slope efficiency. From the modelling, indications were substantiated that the excited state absorption of Cr:LiCAF at higher doping levels is about a factor 1.5 higher compared to the values usually cited for lower doping values, as previously discussed by Isemann and Fallnich [7].

Thus, for the given pump power, Cr:LiSGAF showed the best results in terms of output energy. But scaling to higher pump powers, Cr:LiCAF shows favorable properties as the upper state lifetime of 170 μs allows for efficient energy storage, a high slope efficiency, and the high temperature of 255 °C [6] for the onset of thermal quenching would allow for considerably higher pump powers.

A power scaling was theoretical modelled. The model was verified with the experimental data and applied for scaling the pump power using broad area laser diodes. With an input of 2–4 W of absorbed pump power into the model, Cr:LiCAF showed the highest resultant pulse energy and slope efficiency.

Acknowledgments

References

[1] H. Lubatschowksi, G. Maatz, A. Heisterkamp, U. Hetzel, W. Drommer, H. Welling, W. Ertmer, Graefe's Arch. Clin. Exp. Ophthalmol. 238 (2000) 33.
[2] R. Mellish, N. Barry, S. Hyde, R. Jones, P. French, J. Taylor, C.V. der Poel, A. Valster, Opt. Lett. 20 (22) (1995) 2312.
[3] D. Parsons-Karavassilis, R. Jones, M. Cole, P. French, J. Taylor, Opt. Commun. 175 (2000) 389.
[4] A. Isemann, P. Adel, T. Groß, C. Fallnich, in: OSA Trends in Optics and Photonics (TOPS), vol. 56, Conference on Lasers and Electro-Optics (Cleo2001), Technical Digest, Postconference Edition (Optical Society of America, Washington, DC, 2001), OSA, 2001, p. 501.
[5] F. Balembois, F. Druon, F. Falcoz, P. Georges, A. Brun, Advanced Solid State Lasers, 1997, p. 170.
[6] M. Stalder, M. Bass, B. Chai, J. Opt. Soc. Am. B 9 (12) (1992) 2271.
[7] A. Isemann, C. Fallnich, Opt. Exp. 11 (3) (2003) 259.
[8] U. KellerSemiconductors and Semimetals, vol. 59, Academic Press, New York, 1999, Ch. Semiconductor Nonlinearities for Solid-State Laser Modelocking and Q-Switching.
[9] T. Brabec, C. Spielmann, F. Krausz, Opt. Lett. 16 (24) (1991) 1961.
[10] J. Gordon, J. Opt. Soc. Am. B 9 (1) (1992) 91.
[11] A. Isemann, H. Hundertmark, C. Fallnich, Appl. Phys. B 74 (2002) 299.
[12] V. Pruneri, S. Butterworth, D. Hanna, Opt. Lett. 21 (1996) 390.
[13] D. Strickland, G. Mourou, Opt. Commun. 56 (3) (1985) 219.
[14] A.E. Siegman, Lasers, University Science Books Mill Valey, California, 1986.
[15] A. Isemann, K. Starke, C. Fallnich, H. Welling, in: Advanced Solid-State Lasers, Paper TuB5, OSA Technical Digest (Optical Society of America, Washington, DC), 2001, p. 246.
[16] D. Kopf, J. Aus der Au, U. Keller, G. Bona, P. Roentgen, Opt. Lett. 20 (17) (1995) 1782.
[17] A. Isemann, Diodengepumpte Ultrakurzpuls- und -Verstärkersysteme auf Colquiriite-Basis, Ph.D. Thesis, Universität Hannover, 2002.
[18] C. Rouyer, É. Mazataud, I. Allais, A. Pierre, S. Seznec, C. Sauteret, G. Mourou, A. Migus, Opt. Lett. 18 (3) (1993) 214.
[19] VLOC, Product catalogue and references therein.
[20] R. Mellish, S. Hyde, N. Barry, R. Jones, P. French, J. Taylor, C.V. der Poel, A. Valster, Appl. Phys. B 65 (1997) 221.
[21] L.M. Frantz, J.S. Nodvik, J. Appl. Phys. 34 (8) (1963) 2346.
[22] D. Findlay, R.A. Clay, Phys. Lett. 20 (1966) 277.
[23] I.T. Sorokina, E. Sorokin, E. Wintner, A. Cassanho, H.P. Jenssen, R. Szipocs, OSA TOPS 10 (1997) 322.
[24] P. Beaud, M.C. Richardson, Y.-F. Chen, B.H.T. Chai, IEEE J. Quant. Electron. 30 (5) (1994) 1259.
[25] S.A. Payne, L. Chase, H.W. Newkirk, L.K. Smith, W.F. Krupke, IEEE J. Quant. Electron. 24 (11) (1988) 2243.